

Discretization Uncertainty Estimation based on a Least Squares version of the Grid Convergence Index

Luís Eça and Martin Hoekstra

Abstract

This paper presents the application of a method for the estimation of the discretization uncertainty based on a Least Squares version of the Grid Convergence Index. Grid refinement studies have been performed for two 2-D steady test cases: a Manufactured Solution that mimics a near-wall incompressible turbulent flow and the flow over a backward facing step. The computations were performed with the finite-difference and finite-volume versions of PARNASSOS using the eddy-viscosity one-equation turbulence model of Spalart & Allmaras model and the baseline $k - \omega$ two-equation turbulence model proposed by Menter.

1 Introduction

The significant increase of the use of Computational Fluid Dynamics in engineering applications leads inevitably to a need to establish the credibility of the numerical results. This goal may be achieved with Verification and Validation, which comprise three different stages, [1]:

1. Code Verification.
2. Calculation Verification.
3. Validation.

The first two activities are purely mathematical, whereas the third is a science/engineering activity that intends to assess the suitability of the mathematical model as a representation of the physical problem.

Code Verification aims to verify that a given code solves correctly the equations of the model that it contains by error evaluation. On the other hand, Calculation Verification aims at estimating the error of a given calculation in absence of the exact solution. Verification of Calculations should be preceded by Code Verification and this was one of the main conclusions of the first workshop on uncertainty analysis, held in Lisbon in 2004, [2, 3]. Furthermore, Validation should be performed after Verification (Code and Calculation).

The second Workshop on CFD Uncertainty Analysis is, like its first edition, focused on Calculation Verification. Nevertheless, one of the two test cases is a Manufactured Solution (MS), [4, 5], with the purpose to let all participants demonstrate their code implementation to be bug-free. The intention is to avoid that the results for the physical flow test case (flow over a backward-facing step) are polluted by possible code errors.

In general, the numerical error of a CFD solution includes three components:

- The round-off error, which is a consequence of the finite precision of the computers.

- The iterative error, which is due to the non-linear character of the momentum equations and the transport equations of the turbulence model, as well as the uncoupling of these equations in the solution process.
- The discretization error, being a consequence of the transformation of the continuum equations into a system of algebraic equations.

Normally, the discretization error is the dominant contribution to the numerical error. However, one has to be careful with the round-off error in ill-conditioned problems and with the estimation of the iterative error, [6]. The differences or residuals obtained in the last iteration performed may be two orders of magnitude smaller than the iterative error. And to guarantee a negligible influence of the iterative error, it should be 2 to 3 orders of magnitude smaller than the discretization error, [6].

In this paper we focus on the contribution of the discretization error to the numerical uncertainty (error bar, [7]), after having made sure that the contributions of the round-off and iterative errors are negligible using 15 digits precision and reducing the iterative error to machine accuracy. We have estimated the discretization uncertainty with a procedure based on a least squares version, [8], of the Grid Convergence Index (GCI) proposed by Roache, [1], with an escape to an estimate using the data range when the observed order is found to be outside a certain range.

The two test cases of the second Workshop on CFD Uncertainty Analysis were computed with the finite-difference, [9], and finite volume, [10], versions of PARNASSOS. The calculations were performed with two eddy-viscosity models: the one-equation model proposed by Spalart & Allmaras, [11], and Menter's baseline (BSL) version of the two-equation $k - \omega$ model, [12]. Two slightly different Manufactured Solutions were adopted according to the experience reported in [5]: the MS2 is used for the Spalart & Allmaras model and the MS4 with the BSL $k - \omega$ model. Both solutions have an identical specification of the primary flow variables (velocity and pressure).

Several sets of geometrically similar grids were selected. The purpose of using grids with different geometrical properties is twofold: to verify its role as a source of numerical uncertainty; and to enhance the code verification, because for instance non-orthogonality may activate terms which are inactive on rectangular Cartesian grids. A reasonable number of grids was adopted for each set to allow the application of the least squares version of the GCI.

The paper is organized in the following way: section 2 presents the procedure to estimate the discretization uncertainty; the main properties of the two versions of the PARNASSOS flow solver are summarized in section 3; the results are presented and discussed in section 4; finally, the main conclusions of this study are presented in section 5.

2 Discretization uncertainty estimation

The basis of our procedure for the estimation of the discretization uncertainty U of the solution of an integral or local flow quantity on a given grid is the standard Grid Convergence Index (GCI) method, [1], which says

$$U = F_s |\delta_{RE}|. \quad (1)$$

F_s is a safety factor and δ_{RE} is the error estimation.

The error estimation is preferably obtained by Richardson extrapolation:

$$\delta_{RE} = \phi_i - \phi_o = \alpha h_i^p, \quad (2)$$

where ϕ_i is the numerical solution of any local or integral scalar quantity on a given grid (designated by the subscript i), ϕ_o is the estimated exact solution, α is a constant, h_i is a parameter which identifies the representative grid cell size and p is the observed order of accuracy.

If results on more than three grids are available, ϕ_o , α and p are obtained with a least squares root approach that minimizes the function:

$$S(\phi_o, \alpha, p) = \sqrt{\sum_{i=1}^{n_g} (\phi_i - (\phi_o + \alpha h_i^p))^2}, \quad (3)$$

where n_g is the number of grids available¹. The minimum of $S(\phi_o, \alpha, p)$ is found by setting its derivatives with respect to ϕ_o , p and α equal to zero, [8]. The standard deviation of the fit², U_s , is given by

$$U_s = \sqrt{\frac{\sum_{i=1}^{n_g} (\phi_i - (\phi_o + \alpha h_i^p))^2}{n_g - 3}}. \quad (4)$$

The ability to estimate the error with Richardson extrapolation depends on the apparent convergence condition, being one of the following options:

- Monotonic convergence.
- Oscillatory convergence.
- Monotonic divergence.
- Oscillatory divergence.

Having a single grid triplet with $h_2/h_1 = h_3/h_2$, it is not difficult³ to classify the apparent convergence condition from the convergence ratio:

$$R = \frac{\phi_2 - \phi_1}{\phi_3 - \phi_2},$$

where ϕ_1 stands for the finest grid solution, ϕ_2 for the medium grid and ϕ_3 for the coarsest grid solution. As mentioned by Roache, [7], we have:

$$\begin{aligned} 0 < R < 1 &\Rightarrow \text{Monotonic convergence} \\ -1 < R < 0 &\Rightarrow \text{Oscillatory convergence} \\ R > 1 &\Rightarrow \text{Monotonic divergence} \\ R < -1 &\Rightarrow \text{Oscillatory divergence} \end{aligned}$$

¹If $n_g = 3$, the solution of (3) is equivalent to the solution of (2). Therefore, at least four geometrically similar grids must be available to have a least squares root solution.

²Obviously, the standard deviation of the fit is zero for $n_g = 3$.

³This does not mean that the classification based on a grid triplet is reliable.

When more than three grids are available and the least squares root approach is followed, this classification is not as straightforward, because the data may exhibit scatter, [8]. First, we establish the apparent order of convergence p from the least squares solution of equation (3). Next, to identify the cases of oscillatory convergence or divergence we also determine p^* using $\phi_i^* = |\phi_{i+1} - \phi_i|$ in (3); this fit includes only $n_g - 1$ differences. The apparent convergence condition is then decided as follows:

1. $p > 0$ for $\phi \Rightarrow$ Monotonic convergence.
2. $p < 0$ for $\phi \Rightarrow$ Monotonic divergence.
3. $p^* < 0$ for $\phi^* \Rightarrow$ Oscillatory divergence.
4. Otherwise \Rightarrow Oscillatory convergence.

The only condition which allows an error estimation based on Richardson extrapolation is monotonic convergence. In other cases one must rely on alternative uncertainty quantification, which we have chosen to be based (also) on the maximum difference between all the solutions available, Δ_M ,

$$\Delta_M = \max \left(|\phi_i - \phi_j| \right) \quad \text{with } 1 \leq i \leq n_g \wedge 1 \leq j \leq n_g. \quad (5)$$

In the last few years, we have tested several procedures for the uncertainty estimation based on the GCI using δ_{RE} and Δ_M . The goal is to obtain a error band for a given calculation result such that the exact solution is within that band with 95% confidence. The present version of the procedure is a result of the experience obtained in a variety of test cases and the suggestions and comments of the first Workshop on CFD Uncertainty Analysis held in Lisbon in October 2004, [2]. It starts with the evaluation of the observed order p .

If p is between 1 and 2 we apply the GCI with the proposed safety factor of 1.25. If $p < 1$, δ_{RE} tends to become over-conservative⁴ and so we take the minimum of δ_{RE} and Δ_M as the error estimator.

For super-convergence, i.e. p higher than the theoretical order of the method, the values of δ_{RE} are not reliable. In most of these cases, the observed super-convergence is not real and it is merely a consequence of the numerical shortcomings⁵ affecting the determination of p . If more than 3 grids are available, this is easily identified from the very strong dependence of p on the data points selected. Therefore, in case of super-convergence we perform the Richardson extrapolation with p replaced by its theoretical value to obtain the error estimator. So we introduce δ_{RE}^* , which for a nominally second order method is:

$$\delta_{RE}^* = \phi_i - \phi_o = \alpha h_i^2. \quad (6)$$

Equation (6) is also solved via a least squares approximation by calculating the minimum of

$$S^*(\phi_o, \alpha) = \sqrt{\sum_{i=1}^{n_g} (\phi_i - (\phi_o + \alpha h_i^2))^2}. \quad (7)$$

The uncertainty is obtained from the maximum of the values based on δ_{RE}^* and Δ_M .

⁴ δ_{RE} tends to infinity when p goes to zero.

⁵These shortcomings include the existence of scatter in the data and the possibility of the data being outside the asymptotic range.

In principle, if the code has been verified, i.e. there are no bugs in the implementation of the numerical model, one should not expect to obtain divergent situations, unless the data are outside the asymptotic range. Therefore, in all cases where the data do not exhibit monotonic convergence we determine the uncertainty by multiplying Δ_M with a factor of safety of 3. With our 95% confidence level in mind, this seems an acceptable guess, [2], but requires further corroboration.

We can summarize our procedure for the estimation of the numerical uncertainty, valid for a nominally second-order accurate method, as follows:

1. The observed order of accuracy is estimated with the least squares root technique to identify the apparent convergence condition according to the definition given above.

2. For monotonic convergence:

- For $0.95 \leq p < 2.05$

$$U_\phi = 1.25\delta_{RE} + U_s.$$

- For $0 < p < 0.95$

$$U_\phi = \min(1.25\delta_{RE} + U_s, 1.25\Delta_M).$$

- For $p \geq 2.05$

$$U_\phi = \max(1.25\delta_{RE}^* + U_s, 1.25\Delta_M)$$

3. If monotonic convergence is not observed:

$$U_\phi = 3\Delta_M$$

The procedure assumes the iterative and round-off errors to be negligible, and the data to be in the so-called asymptotic range (to justify the use of (2)). This implies typically the use of highly refined grids. But with the increase of the grid density it may be more difficult to ensure that the iterative error is negligible and it also enhances the role of the round-off error. Therefore, in practice, it is not possible to increase the grid density indefinitely in a grid refinement study.

3 PARNASSOS flow solver

The 2-D versions of PARNASSOS solve the steady, incompressible, Reynolds-averaged Navier Stokes equations using eddy-viscosity turbulence models. Details of the implementation of the two versions are given in [9] and [10]. The main properties of the two versions are summarized below.

- The finite-difference, FD, version discretizes the continuity and momentum equations written in Contravariant form, which is a weak conservation form. The finite-volume, FV, version discretizes the strong conservation form of the equations.
- The FD version computes the momentum balance along the directions of the curvilinear coordinate system, whereas the FV version calculates the momentum balance for its Cartesian components.

- The FD code has a fully-collocated arrangement with the unknowns and the discretization centered at the grid nodes. In the FV code unknowns are defined at cell centres.
- Both versions apply quasi-Newton linearization to the convective terms and are at least second order accurate for all the terms of the continuity and momentum equations. Third-order upwind discretisation is applied to the convective terms.
- The linear system of equations formed by the discretized continuity and momentum equations is in both versions solved simultaneously, using GMRES, [13], with a coupled ILU preconditioning.
- Under-relaxation is applied with a quasi time-derivative term.
- The transport equations for the turbulence quantities are discretized with first or third-order (with or without limiters) upwind schemes.
- The linearization procedure of the production and dissipation terms of the turbulence quantities follows the standard approach, i.e. production is added to the right-hand side and dissipation to the main-diagonal.
- The solution of the turbulence quantities transport equations is uncoupled from solving the continuity and momentum equations.

4 Calculation of the Manufactured Solution

The proposed MS is defined in a squared domain ($0.5 \leq x \leq 1$ and $0 \leq y \leq 0.5$) using dimensionless variables and L and U_{ref} as the reference length and velocity. x and y are the Cartesian horizontal and vertical coordinates, respectively. The horizontal and vertical velocity components are designated by u_x and u_y and the pressure coefficient is defined by

$$C_p = \frac{p}{\rho U_{ref}^2}.$$

The Reynolds number is

$$Re = \frac{U_{ref} L}{\nu} = 10^6.$$

The MS2, [5], was adopted for the calculations performed with the Spalart & Allmaras one-equation, whereas MS4, [4], was used in the calculations performed with the BSL $k - \omega$ two-equation model.

One of the advantages of the MMS is its flexibility to test different parts of the code. Although the main goal is to compute the complete flow field, it is instructive to perform three different exercises with the proposed MS:

1. Calculate the flow field with the manufactured eddy-viscosity.
2. Calculate the eddy-viscosity field with the manufactured velocity field.

3. Calculate the complete flow field.

The first two exercises are relevant to assess the numerical properties of the flow solver. In the first case, the solution of the continuity and momentum equations with the manufactured eddy-viscosity, one may expect to obtain the theoretical order of the schemes applied in the discretization of the equations. However, the turbulence quantities transport equations are usually non-linear equations including damping functions and so it is not guaranteed that one recovers all the expected numerical properties of the solution of linear equations.

As illustrated in [14], a first-order scheme in the turbulence quantities transport equations may lead to a first-order convergence of the mean flow variables. Therefore, we have adopted the third-order upwind scheme for the discretization of the convective terms in the transport equations of the turbulence quantities.

The observed order of accuracy, p , of all the flow variables is estimated with the least squares root approach applied to the 11 finest grids of each set that cover a grid refinement ratio of 2.

4.1 Boundary Conditions

The boundary conditions applied in the calculation of the proposed MS are similar to the typical boundary conditions of a boundary-layer calculation.

- The velocity components and the vertical pressure derivative are fixed from the MS at the bottom boundary.

$$u_x = (u_x)_{ms} = 0, \quad u_y = (u_y)_{ms} = 0, \quad \frac{\partial C_p}{\partial y} = \left(\frac{\partial C_p}{\partial y} \right)_{ms} = 0.$$

The turbulence quantities are also specified from the manufactured solution. This is straightforward for $\tilde{\nu}$ and k ($\tilde{\nu} = 0$ and $k = 0$), but not for ω that tends to infinity at the wall. To avoid problems caused by the specified ω at the wall, we have imposed ω from the MS at the first two nodes away from the wall.

- At the inlet boundary, the velocity components and the horizontal pressure derivative are fixed from the MS.

$$u_x = (u_x)_{ms}, \quad u_y = (u_y)_{ms}, \quad \frac{\partial C_p}{\partial x} = \left(\frac{\partial C_p}{\partial x} \right)_{ms}.$$

All the turbulence quantities are specified from the MS.

- u_x and C_p are fixed at the top boundary.

$$u_x = (u_x)_{ms}, \quad C_p = (C_p)_{ms}.$$

In the finite-difference version, the continuity equation is solved at the top boundary to obtain u_y . In the finite-volume version, the second derivative of u_y with respect to y is set equal to the value taken from the MS.

$$\frac{\partial^2 u_y}{\partial y^2} = \left(\frac{\partial^2 u_y}{\partial y^2} \right)_{ms}.$$

All the turbulence quantities are specified from the MS.

- The derivatives of the velocity component with respect to x and the pressure coefficient are taken from the MS at the outlet boundary.

$$\frac{\partial u_x}{\partial x} = \left(\frac{\partial u_x}{\partial x} \right)_{ms}, \quad \frac{\partial u_y}{\partial x} = \left(\frac{\partial u_y}{\partial x} \right)_{ms}, \quad C_p = (C_p)_{ms}.$$

Neumann boundary condition are applied to all the turbulence quantities with the normal derivative taken from the MS.

4.2 Grid Sets

We have selected four sets of 20 geometrical similar grids to perform the calculations of the proposed Manufactured Solution:

- Set A includes equally-spaced grids.
- Set B has Cartesian grids with uniform spacing in the x direction and clustered nodes close to the bottom. The one-sided stretching functions proposed by Vinokur, [15], were applied using a stretching parameter of 0.05 (first spacing is 0.05 times the equally-spaced grid).
- Set C includes non-orthogonal curvilinear grids with a mean deviation from orthogonality of 14.1° degrees and a maximum deviation from orthogonality of 44.1° degrees. The grid lines are orthogonal at the boundaries. One family of grid lines is identical to the horizontal lines of set B and the other family is obtained with Hermite polynomials that connect the bottom and top boundaries.
- Set D has the same boundary point distribution of set C. However, the boundary orthogonality is lost because the Hermite interpolations have been replaced by linear interpolations. In this case the mean deviation from orthogonality is 21.2° degrees and the maximum deviation from orthogonality 33.1° degrees.

The finest grid of each set contains 401×401 nodes and the coarsest 101×101 covering a grid refinement ratio of 4. For illustration purposes, the 21×21 grids of each set are depicted in figure 1.

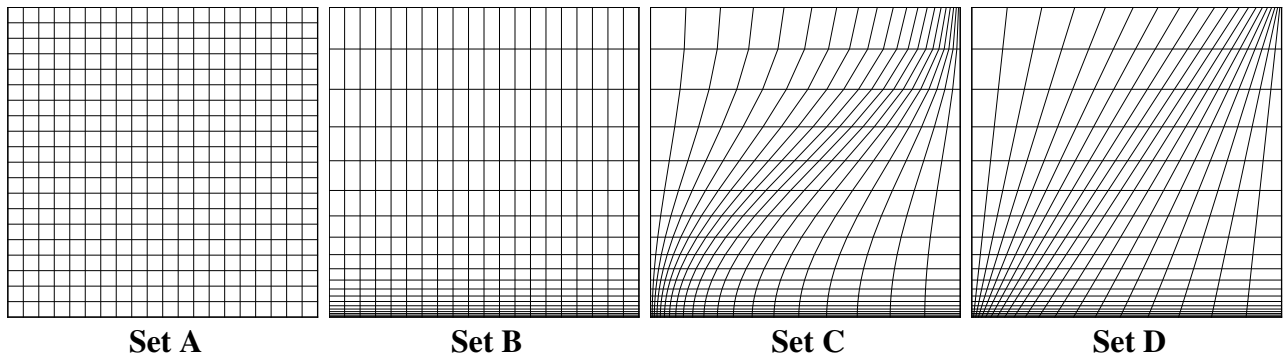


Figure 1: Illustration of the four grids sets for the calculation of Manufactured Solution.

4.3 Calculation of the flow field with the Manufactured eddy-viscosity field

The first exercise performed was the calculation of the velocity and pressure field with the manufactured eddy-viscosity, ν_t . In the MS2 solution, ν_t is the manufactured dependent variable of the Spalart & Allmaras model, $\tilde{\nu}$, multiplied by the damping function of the model.

Table 1 presents the observed order of accuracy, p , of the root mean square (RMS) error of u_x , u_y , and C_p in the MS4 and MS2 solutions for the four grid sets selected. p was estimated with the least squares root approach applied to the 11 finest grids of each set that cover a grid refinement ratio of 2. As an example, figure 2 presents the RMS error of u_x as a function of the grid refinement ratio, h_i/h_1 , where h is the typical cell size.

Grid Set	Finite-Differences						Finite Volume					
	MS2			MS4			MS2			MS4		
	u_x	u_y	C_p	u_x	u_y	C_p	u_x	u_y	C_p	u_x	u_y	C_p
A	0.5	—	—	2.0	2.0	2.0	4.3	—	—	2.0	2.1	2.1
B	2.0	2.0	2.0	2.0	2.0	2.0	2.0	2.0	2.0	2.0	2.0	2.0
C	2.0	2.0	2.0	2.0	2.0	2.0	2.0	2.0	2.0	2.0	2.0	2.0
D	2.0	2.0	2.0	2.0	2.0	2.0	2.0	2.0	2.0	2.0	2.0	2.0

Table 1: Observed order of accuracy of the RMS error of u_x , u_y , and C_p . Calculations performed with the manufactured eddy-viscosity.

The three grid sets with clustered grid nodes close to the bottom (sets B, C and D) lead to the expected behaviour for the three flow variables with $p = 2.0$ and very similar levels of error. However,

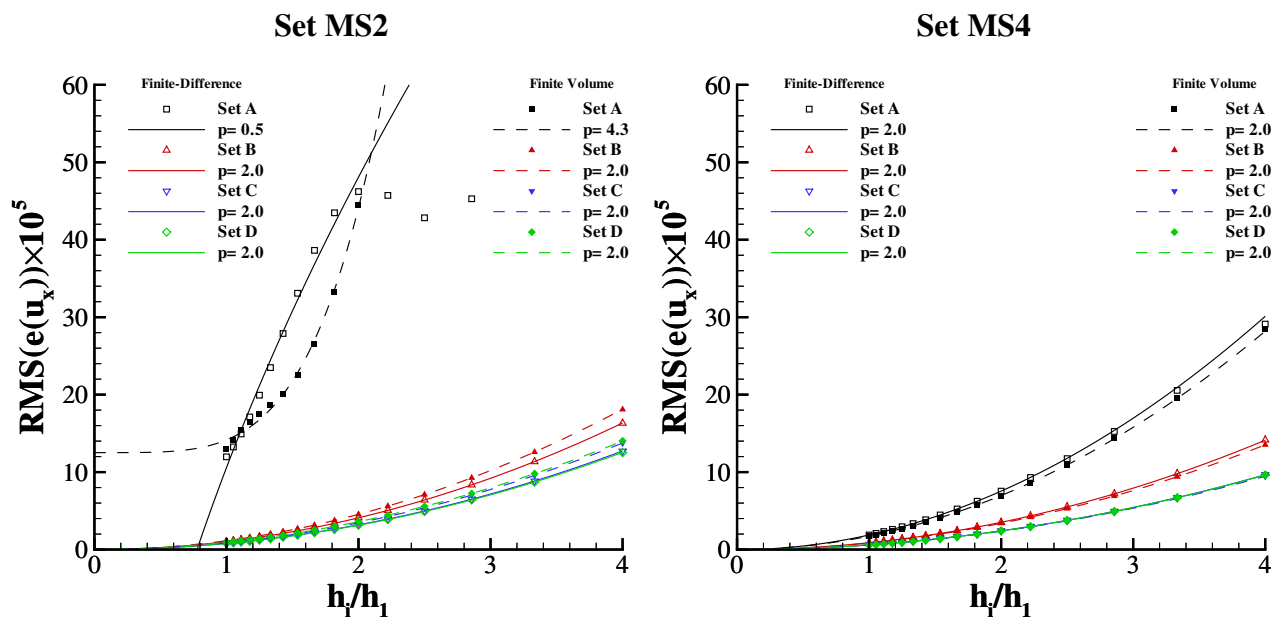


Figure 2: RMS of the error of u_x as a function of the grid refinement ratio. Calculations performed with the manufactured eddy-viscosity.

the equally-spaced grids exhibit an interesting result: the convergence of the MS4 solution has the expected p with a reasonable increase of the error compared with the other grid sets; the MS2 solution is clearly outside the so-called "asymptotic range" and the error level is 10 times larger than in the MS4 solution. This is a remarkable result originated by the change in the level of the eddy-viscosity in the "near-wall" region. This is illustrated in figure 3 that presents the two eddy-viscosity profiles at $x = 0.75$.

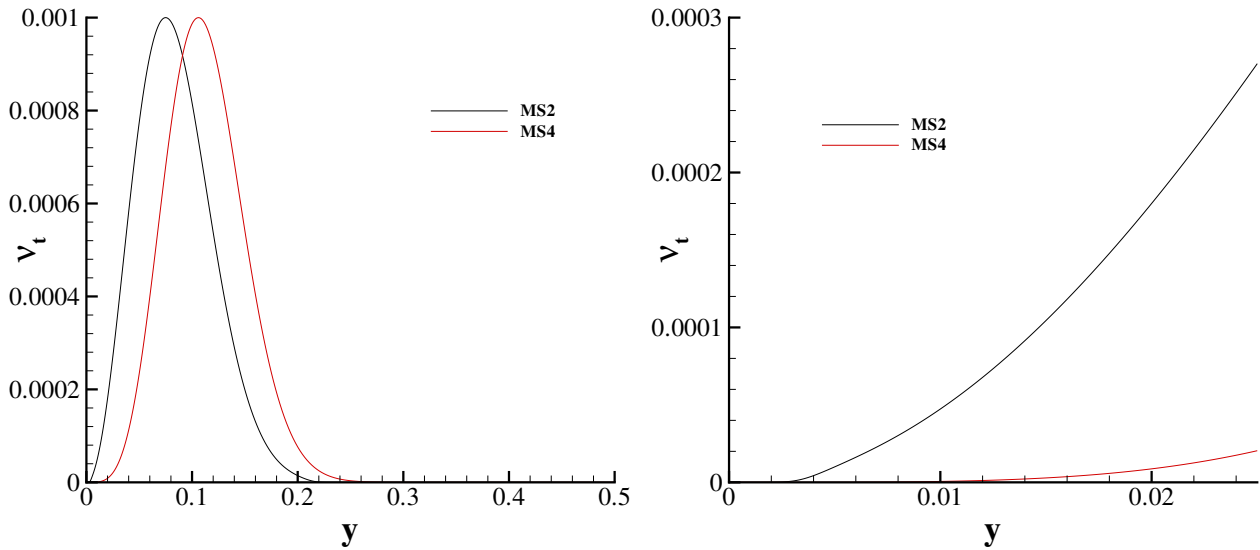


Figure 3: Manufactured eddy-viscosity profiles at $x = 0.75$.

4.4 Calculation of the eddy-viscosity field with the Manufactured velocity field

One of the advantages of the MMS is that it allows the investigation of the numerical properties of the turbulence quantities transport equations using the manufactured velocity field. This is an important exercise because most of the transport equations proposed by the turbulence models include non-linear terms. In fact, the transport equations of the two turbulence models selected do not include a single linear term.

Table 2 presents the observed order of accuracy of the RMS error of the turbulence quantities included in the two turbulence models: \tilde{v} and v_t for the Spalart & Allmaras model; v_t , k and ω for the BSL $k - \omega$ model. Due to the fact that ω goes to infinity at the bottom, the RMS error of ω increases with the grid refinement, [16]. Therefore, we have also computed the RMS error of ωy^2 (that remains finite at the wall) for the BSL model.

4.4.1 Spalart & Allmaras model

Figure 4 illustrates the convergence of \tilde{v} and v_t with the grid refinement for the calculation performed with the MS2 solution.

Grid Set	Finite-Differences						Finite Volume					
	MS2		MS4				MS2		MS4			
	\tilde{v}	v_t	\tilde{v}	v_t	v_t	k	ω	ωy^2	v_t	k	ω	ωy^2
A	2.0	2.0	1.6	1.7	—	2.3	1.7	1.9	1.8	1.9	—	2.1
B	2.0	2.0	1.7	1.9	—	2.0	2.0	2.0	1.9	1.9	—	2.0
C	2.0	2.0	1.8	1.9	—	2.0	2.0	2.0	1.9	2.0	—	1.9
D	2.0	2.0	1.8	1.9	—	2.0	2.0	2.0	1.9	2.0	—	2.1

Table 2: Observed order of accuracy of the RMS error of \tilde{v} , and v_t . Calculations performed with the manufactured velocity field.

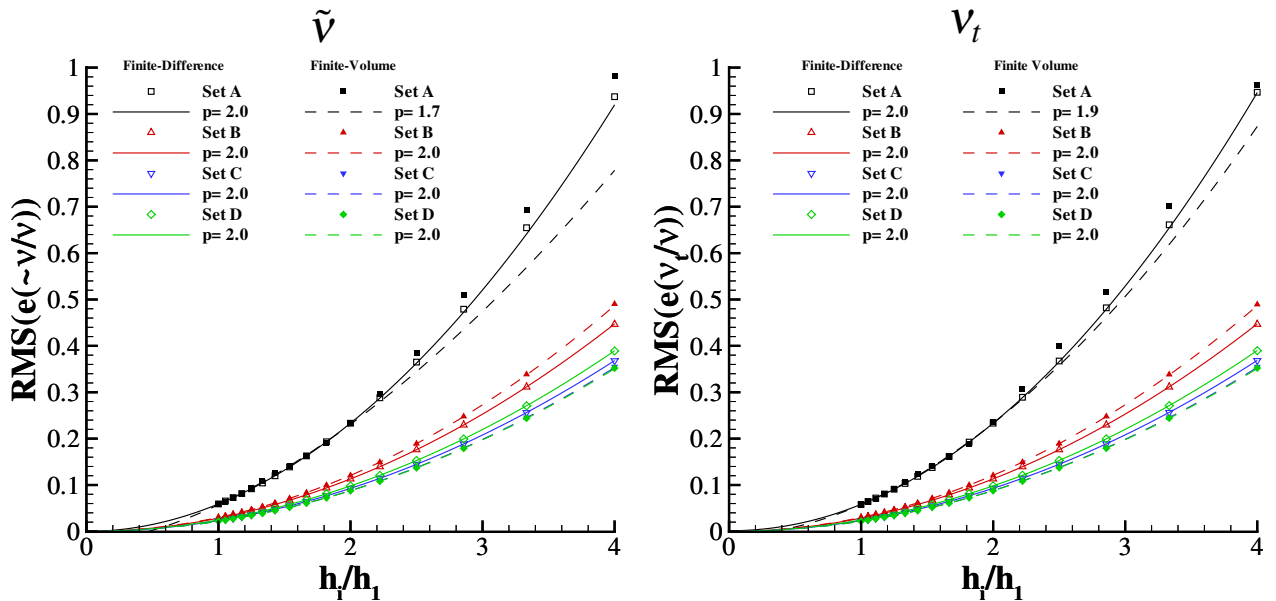


Figure 4: RMS of the error of \tilde{v} and v_t as a function of the grid refinement ratio. Spalart & Allmaras model with the MS2 solution using the manufactured velocity field.

The results obtained for the turbulence quantities of the Spalart & Allmaras model exhibit the theoretical order of accuracy for 7 of the 8 cases tested. The single exception is the equally-spaced grids set with the finite volume code where the observed p is slightly below 2. It is remarkable to see that \tilde{v} and v_t do not show the convergence problems observed in grid set A for u_x , u_y and C_p in the previous exercise. It is also important to emphasize that the data obtained for set A illustrate once more the difficulties to determine the observed order of accuracy. The results obtained with the two versions of PARNASSOS are slightly different but the estimated value of p differs 0.3 for \tilde{v} .

4.4.2 BSL $k - \omega$ model

Figure 4 presents the convergence of v_t , k , ω and ωy^2 with the grid refinement for the calculation performed for the BSL $k - \omega$ model with the MS4 solution. The results yield an observed order of accuracy between 1.6 and 2.0 for v_t and k . However for the three grid sets with clustering of grid

lines close to the bottom p is equal to 1.9 or 2.0.

As expected, the RMS error of ω increases with the grid refinement due to the ω wall boundary condition. The equally-spaced grid, which exhibits the largest near-wall spacing, shows the smallest level of error for ω , but for the finest grids the increase of the error with the grid refinement is already visible. The finite volume solutions present a larger error level than the finite-difference, because the unknowns are collocated at the centre of the cells and so the first node where ω is determined is closest to the wall in the finite volume version.

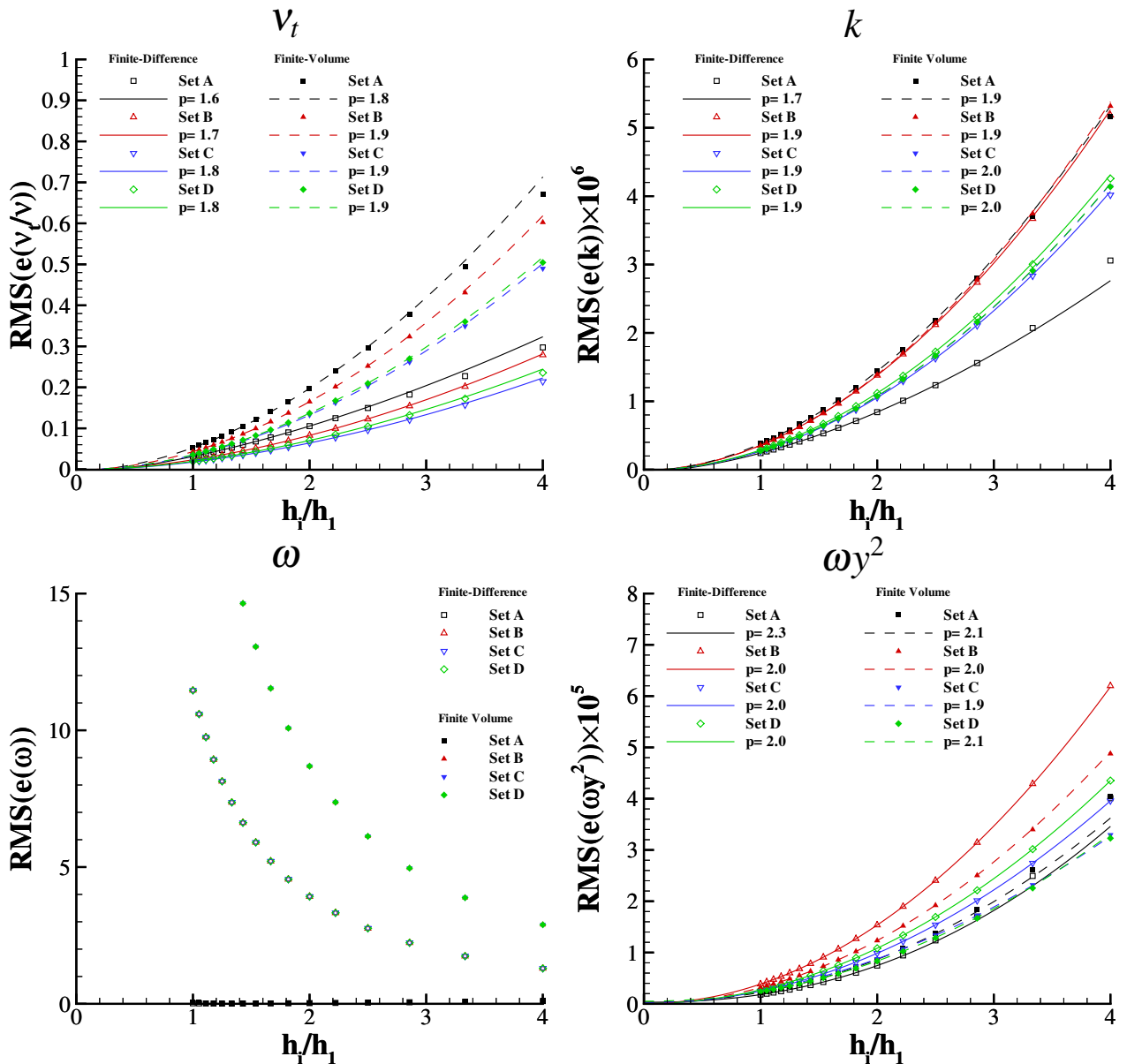


Figure 5: RMS of the error of v_t , k , ω and ωy^2 as a function of the grid refinement ratio. BSL $k - \omega$ model with the MS4 solution using the manufactured velocity field.

The convergence of ωy^2 shows that the problems of the wall boundary condition are a local effect. In all the solutions, ωy^2 converges with the grid refinement with observed order of accuracy between

1.9 and 2.1, whereas the RMS error of ω increases significantly with the grid refinement for grid sets B, C and D.

4.5 Calculation of the complete flow field

The final exercise performed with the manufactured solutions is the calculation of the complete flow field. One could expect the same behaviour obtained in the previous exercises. However, that is not guaranteed because the relation between the momentum equations and the eddy-viscosity and between the transport equations of the turbulence model and the velocity field is not linear.

In this case, we have also computed the friction resistance coefficient at the bottom wall

$$C_D = 2 \frac{\int_{0.5}^1 \nu \left(\frac{\partial u_x}{\partial y} \right)_{y=0}}{U_{ref}^2}$$

4.5.1 Spalart & Allmaras model

The calculation of the MS2 solution with the Spalart & Allmaras model is rather time consuming. For both versions of the code, the reduction of the iterative error to machine accuracy requires more than 2000 iterations for all the grids tested. The problem is related to the non-linearity of the system of equations, because the solution of the linear systems of equations of each iteration converges without any problems.

Although we have not investigated exhaustively all the possible origins of the slow convergence of the iterative error, the results of the previous exercises indicate that the problem is originated by the transport equation of the turbulence model. The calculations performed with the manufactured eddy-viscosity converge to machine accuracy in no more than 250 iterations, whereas the calculation of the turbulence model transport equation with the manufactured velocity field requires 5 times more iterations (but not too much c.p.u. time) to converge the solution to machine accuracy. We have only performed the complete flow field calculation with the two versions of the code for grid set B.

Table 3 presents the observed order of accuracy of the RMS error of u_x , u_y , C_p , v_t and $\tilde{\nu}$. The observed order of accuracy of C_D is also included in table 3. The convergence of the RMS error of u_x and C_D with the grid refinement is presented in figure 6 and the convergence of the turbulence quantities is illustrated in figure 7.

Set	Finite-Differences						Finite Volume					
	u_x	u_y	C_p	v_t	$\tilde{\nu}$	C_D	u_x	u_y	C_p	v_t	$\tilde{\nu}$	C_D
B	1.3	1.1	1.1	1.5	1.5	1.6	2.3	2.3	2.3	2.1	2.1	2.6

Table 3: Observed order of accuracy of the RMS error of u_x , u_y , C_p , v_t , $\tilde{\nu}$ and C_D . Complete flow field calculations for the MS2 with the Spalart & Allmaras turbulence model.

None of the flow variables exhibits the observed order of accuracy, which is in contrast with the results obtained for the two previous exercises. It is interesting to remark that the finite-difference

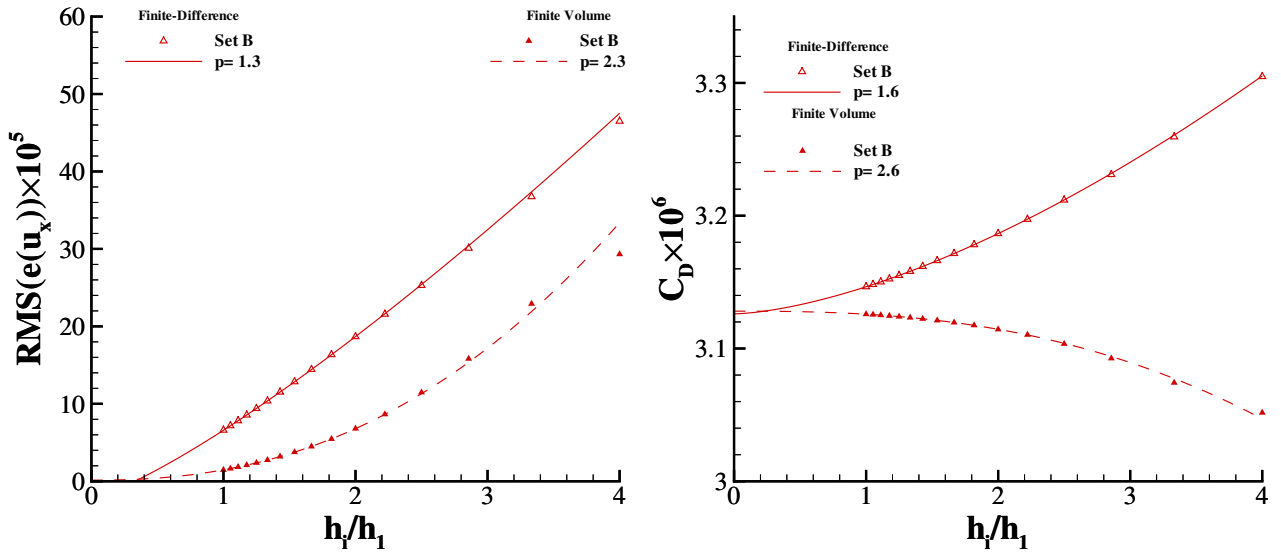


Figure 6: RMS of the error of u_x and C_D as a function of the grid refinement ratio. Complete flow field calculations for the MS2 with the Spalart & Allmaras turbulence model.

version leads consistently to p below 2 and the finite volume to p above 2. In general, the observed order of accuracy tends to 2 (but does not reach 2) if we consider only the 4 finest grids of the set. Therefore, the results suggest that we have not attained the asymptotic range even with grids of more than 341×341 grid nodes.

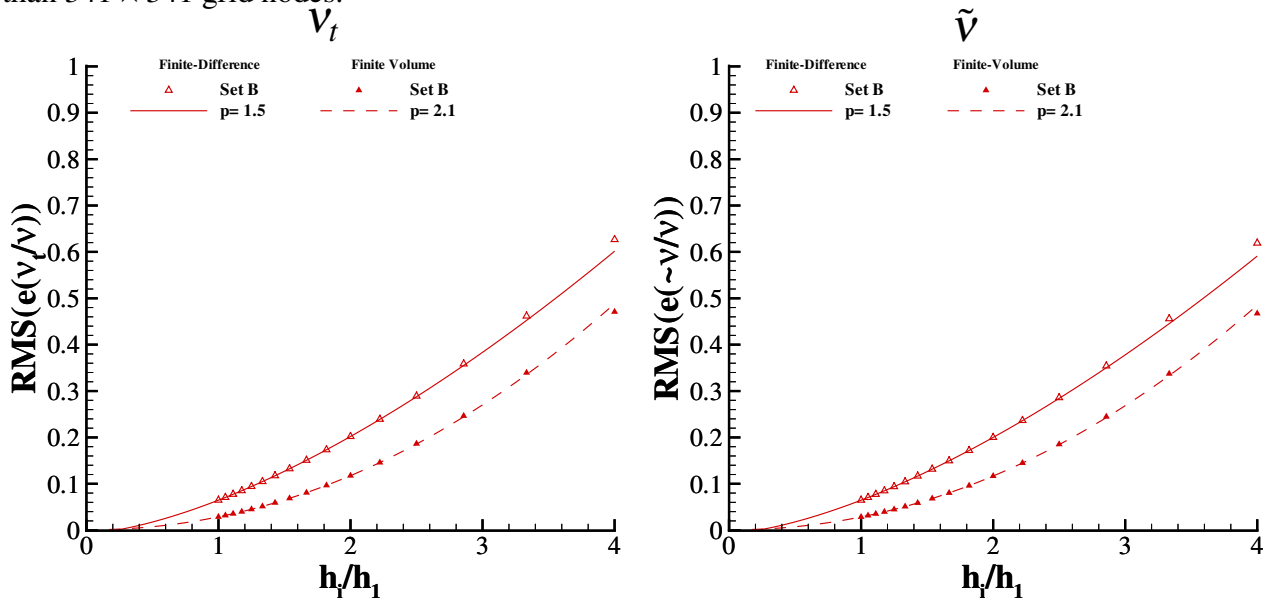


Figure 7: RMS of the error of v_t and \tilde{v} as a function of the grid refinement ratio. Complete flow field calculations for the MS2 with the Spalart & Allmaras turbulence model.

As an example of local flow quantities convergence, figure 8 presents the convergence of u_x with the grid refinement at the three selected locations for the Workshop: $x = 0.6, y = 0.001$, $x = 0.6, y = 0.001, x = 0.75, y = 0.002$ and $x = 0.9, y = 0.2$. It is clear that u_x at the two locations closest to the wall (where the damping function of the turbulence model is active) shows a less smooth convergence than

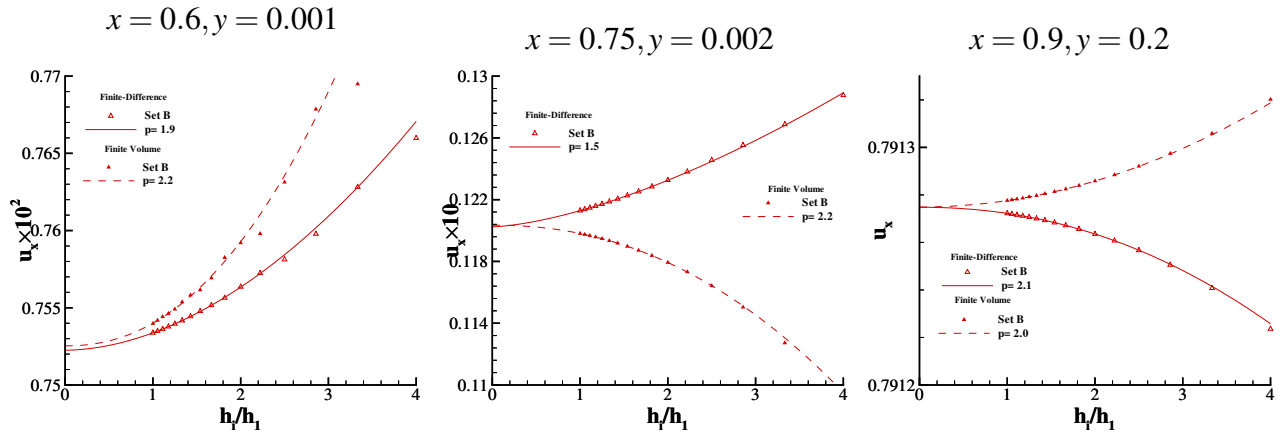


Figure 8: Convergence of u_x as a function of the grid refinement ratio at $x = 0.6, y = 0.001$, $x = 0.75, y = 0.002$ and $x = 0.9, y = 0.2$. Complete flow field calculations for the MS2 with the Spalart & Allmaras turbulence model.

u_x at $x = 0.9, y = 0.2$. Furthermore, the data obtained in the coarsest grids shows also some scatter at $x = 0.6, y = 0.001$, which was not present in any of the previous exercises.

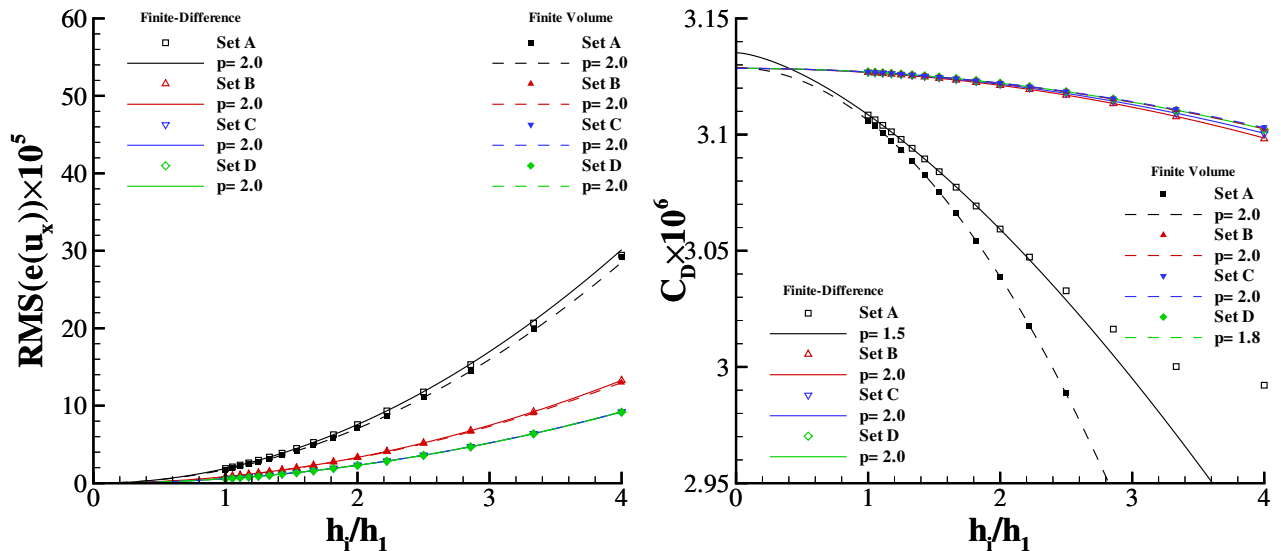


Figure 9: RMS of the error of u_x and C_D as a function of the grid refinement ratio. Complete flow field calculations for the MS4 with the BSL $k - \omega$ turbulence model.

4.5.2 BSL $k - \omega$ model

With the BSL $k - \omega$ model we have performed calculations for the 4 grid sets with the two versions of the code. The observed order of accuracy of the RMS error of u_x , u_y , C_p , v_t , k , ω , and ωy^2 are presented in table 4. The observed order of accuracy of C_D is also included in table 4. The convergence of the RMS error of u_x and C_D with the grid refinement is presented in figure 9 and the convergence of the turbulence quantities is illustrated in figure 10.

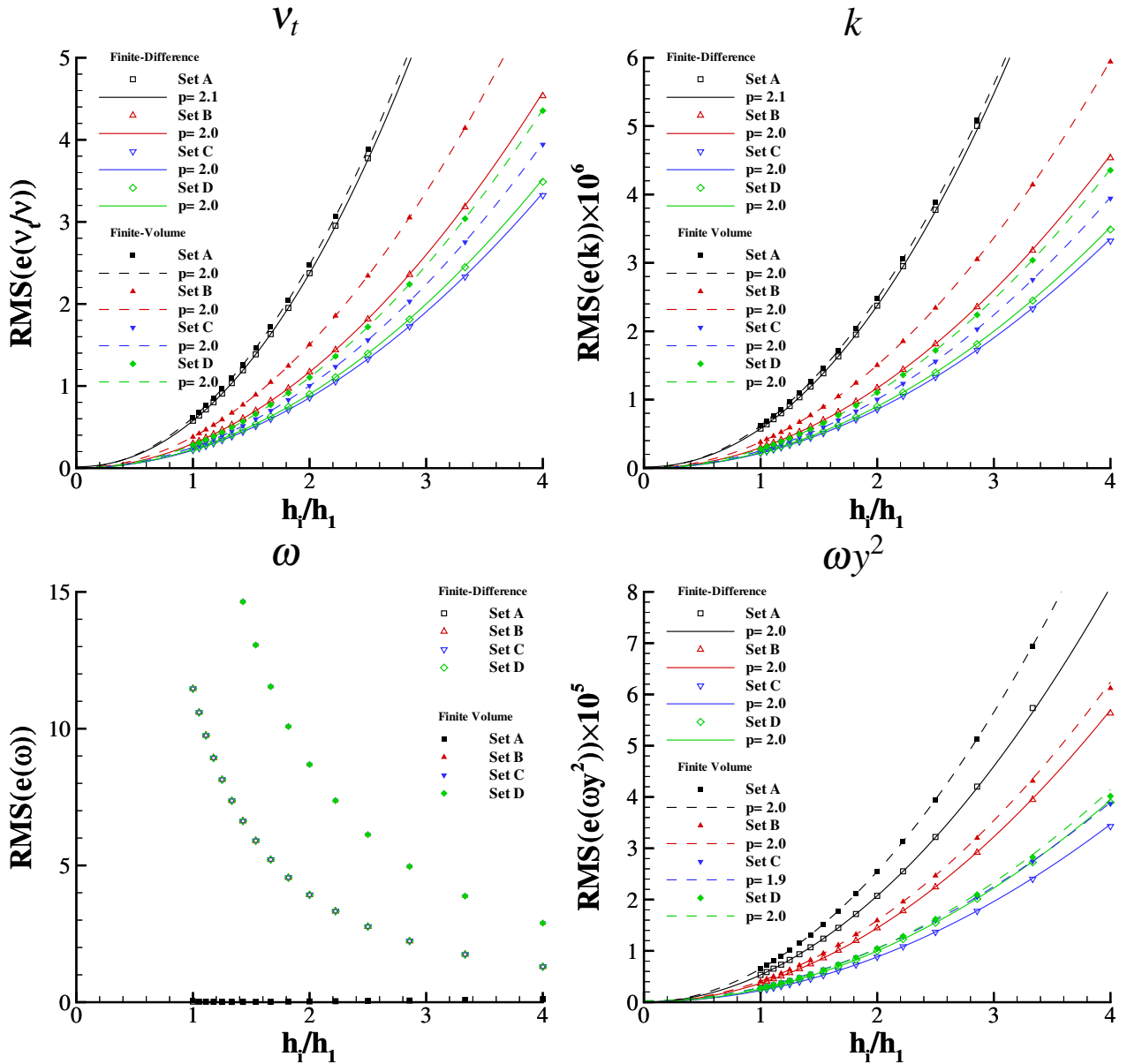


Figure 10: RMS of the error of v_t , k , ω and ωy^2 as a function of the grid refinement ratio. Complete flow field calculations for the MS4 with the BSL $k - \omega$ turbulence model.

Set	Finite-Differences								Finite Volume							
	u_x	u_y	C_p	v_t	k	ω	ωy^2	C_D	u_x	u_y	C_p	v_t	k	ω	ωy^2	C_D
A	2.0	2.0	2.0	1.9	2.1	—	2.0	1.5	2.0	2.0	2.1	1.9	2.0	—	2.0	2.0
B	2.0	2.0	2.0	1.8	2.0	—	2.0	2.0	2.0	2.0	2.0	1.9	2.0	—	2.0	2.0
C	2.0	2.0	2.0	1.9	2.0	—	2.0	2.0	2.0	2.0	2.0	1.9	2.0	—	1.9	2.0
D	2.0	2.0	2.0	1.9	2.0	—	2.0	2.0	2.0	2.0	2.0	1.9	2.0	—	2.0	1.8

Table 4: Observed order of accuracy of the RMS error of u_x , u_y , C_p , v_t , k , ω , ωy^2 and C_D . Complete flow field calculations for the MS4 with the BSL $k - \omega$ turbulence model.

With the BSL $k-\omega$ model, the observed order of accuracy of the RMS error of all the selected flow quantities (with the obvious exception of ω) is close to 2. Furthermore, the error level is equivalent to the one obtained in the previous exercises. Although ω tends to infinity at the wall, the observed order of accuracy of C_D is 2. However, it should be mentioned that in the present calculations ω is specified from the MS at the first two nodes (cells) away from the wall.

As an example of the convergence of local flow quantities, figure 10 presents the convergence u_x with the grid refinement at $x = 0.6, y = 0.001$ and $x = 0.75, y = 0.002$. The effect of the selected grid spacing is clear in the convergence of u_x at the two locations closest to the wall. It is important to emphasize that even in a flow quantity where the RMS of the error is converging with the theoretical order of the method, there are locations where the observed order of accuracy is not equal to 2.

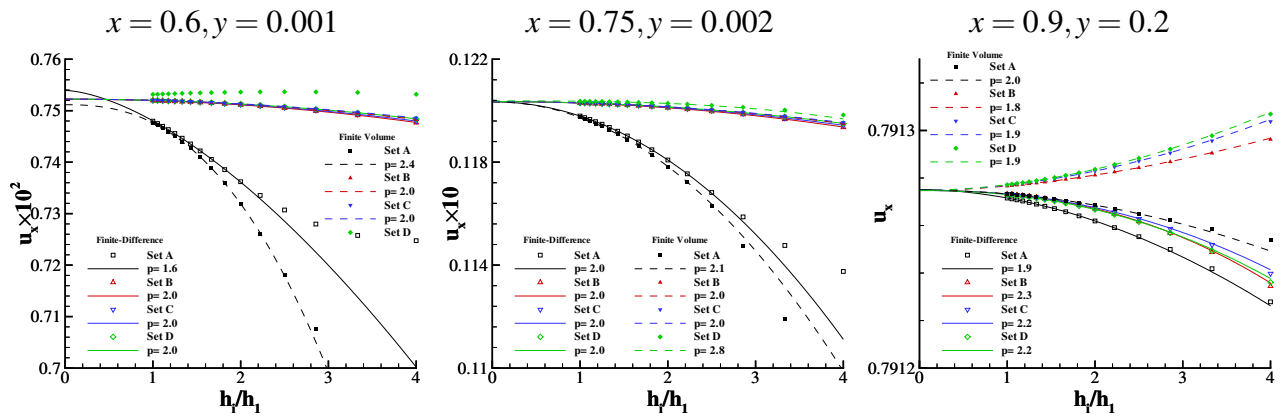


Figure 11: Convergence of u_x as a function of the grid refinement ratio at $x = 0.6, y = 0.001$, $x = 0.75, y = 0.002$ and $x = 0.9, y = 0.2$. Complete flow field calculations for the MS4 with the BSL $k-\omega$ turbulence model.

5 Calculation of the flow over a backward facing step

The computational domain of the flow around a backward facing step is bounded by two walls and two x constant planes $-4h$ upstream and $40h$ downstream of the step, where h is the step height. The Reynolds number based on the step height and the velocity of the incoming flow is 5×10^5 .

With the finite-difference (FD) version of the code, we have performed calculations with the Spalart & Allmaras and BSL $k-\omega$ model using first (C1) and third-order (C3) upwind in the convective terms of the turbulence quantities transport equations. With the finite volume version (FV), the calculations were performed with the Spalart & Allmaras model using limiters (LM) for the convective terms of the momentum equations and turbulence quantities transport equations.

In the present paper we will focus on the flow quantities selected for the 2nd Workshop on CFD Uncertainty Analysis. The discretization uncertainty is estimated for the finest grid of each set using the grids that cover a grid refinement ratio of 2. Obviously, the number of cases where it is possible to estimate p will increase if we select the number of grids to estimate the observed order of accuracy for each flow variable. However, such approach is not practical. Furthermore, the present procedure

	Version	Set	Turbulence Model	Convection discretization
1	FD	A	Spalart & Allmaras	First-order in the \tilde{v}_t equation
2	FD	A	Spalart & Allmaras	Third-order in the \tilde{v}_t equation
3	FD	B	Spalart & Allmaras	First-order in the \tilde{v}_t equation
4	FD	B	Spalart & Allmaras	Third-order in the \tilde{v}_t equation
5	FD	A	BSL $k - \omega$	First-order in the k and ω equations
6	FD	A	BSL $k - \omega$	Third-order in the k and ω equations
7	FD	A	BSL $k - \omega$	First-order in the k and ω equations
8	FD	A	BSL $k - \omega$	Third-order in the k and ω equations
9	FV	C	Spalart & Allmaras	Third-order with limiters in all transport equations.

Table 5: Designation of the calculations performed for the backward facing step.

to estimate the discretization uncertainty is supposed to take care of situations where it is not possible to estimate p .

5.1 Boundary Conditions

In the present calculations we have specified all the required flow quantities at the inlet, with the exception of the pressure coefficient, using the profiles generated for the Workshop, [2]. The pressure coefficient is extrapolated from the interior of the domain, assuming that its second derivative in the streamwise direction is zero.

At the walls, the no-slip and impermeability conditions are applied, which leads to $u_x = u_y = 0$. \tilde{v} and k are set equal to 0 and ω is specified at the first two nodes away from the wall using the near wall solution of the ω transport equation proposed by Wilcox, [17].

In the finite-difference version of the method, the momentum equation in the normal direction is solved at the wall to obtain the pressure value; in the finite volume version the pressure at the wall is found from linear extrapolation from the interior of the domain.

u_x , u_y and the turbulence quantities are linearly extrapolated from the interior of the domain. The pressure coefficient is set to zero.

5.2 Grid Sets

We have selected two sets of 8 and one of 7 single-block, structured, geometrically similar grids to perform the calculations of the flow over a backward facing step.

- Set A is similar to the first grid set proposed for the first edition of the Workshop, [2], containing non-orthogonal curvilinear grids with the same number of nodes in both directions. At the walls the grids are orthogonal. However, the grids no longer have kinks at the interior grid lines coming from the corners of the step.

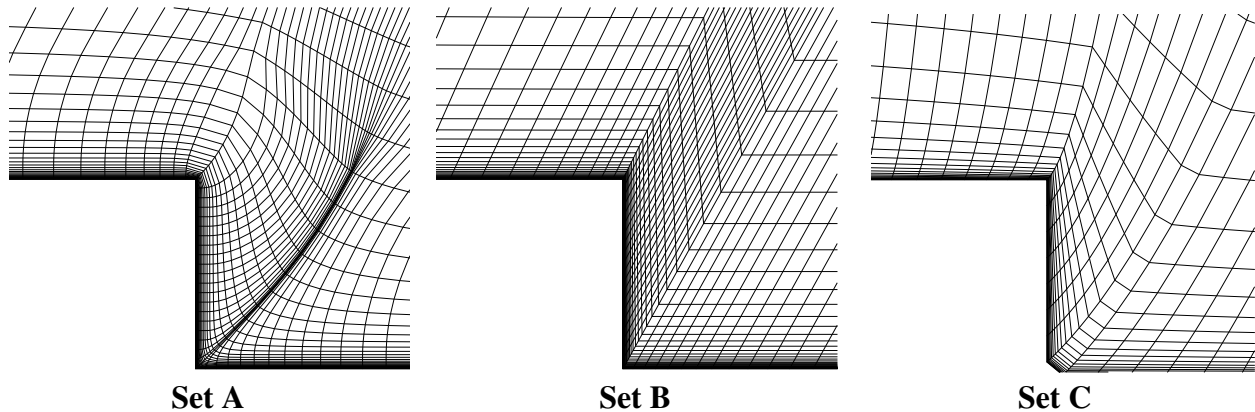


Figure 12: Illustration of the three grids sets for the calculation of the flow over a backward facing step.

- Set B is the same as the set B proposed for the first edition of the Workshop, [2], which includes straight lines connecting the bottom and top walls and the same number of nodes in both directions.
- Set C includes non-orthogonal curvilinear grids with the number of nodes in the streamwise direction equal to the double of the number of nodes in the normal direction. As opposed to grid set A the grid lines are not everywhere normal to the walls.

The finest grid of sets A and B contains 241×241 nodes and the coarsest 101×101 covering a grid refinement ratio of 2.4. The finest grid of set C includes 401×201 nodes and the coarsest one 161×81 covering a grid refinement ratio of 2.5. Figure 12 illustrates the 101×101 and 101×51 (not included in the calculations) of the three grid sets in the vicinity of the step.

5.3 u_x , horizontal velocity component

Figure 13 presents the results obtained for the horizontal velocity component, u_x , at the three selected locations: $x = 0, y = 1.1h$, $x = h, y = 0.1h$ and $x = 4h, y = 0.1h$. The plots include the convergence with the grid refinement and the error bars estimated for the finest grid of each set.

The data show that for the present level of grid refinement it is difficult to establish the observed order of accuracy. There are no cases with $p=2$ and there are a few grid sets where it is not possible to obtain the value of p from the selected grids. As a consequence, the estimated uncertainty is mostly obtained from three times the data range and it is probably too conservative. Nevertheless, the error bars at $x = 4h, y = 0.1h$ for the Spalart & Allmaras model do not show complete overlap for the 5 calculations performed.

In general, the estimated uncertainty is larger for the BSL $k - \omega$ model than for the Spalart & Allmaras model. There is no reduction of the estimated error bar for the C3 calculations when compared with the C1. Comparison with the data behaviour in the MS suggests that the present level of grid refinement is clearly outside the asymptotic range.

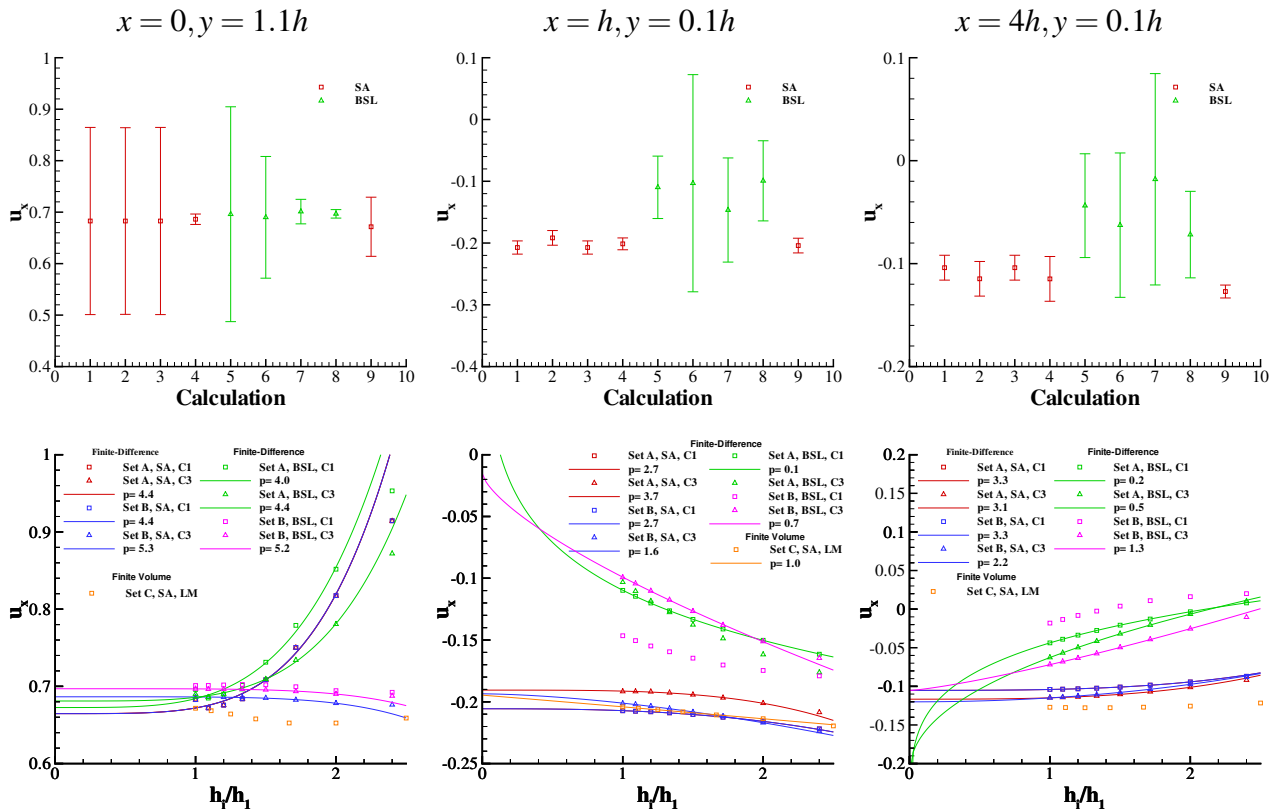


Figure 13: Convergence of u_x as a function of the grid refinement ratio at $x = 0, y = 1.1h$, $x = h, y = 0.1h$ and $x = 4h, y = 0.1h$ and respective error bars. Flow over a backward facing step.

5.4 u_y , vertical velocity component

The convergence of the vertical velocity component, u_y , with the grid refinement and the error bars at the three selected locations are presented Figure 14.

The number of cases where it is not possible to obtain p is clearly larger than for u_x . At $x = 0, y = 1.1h$ there are several grid sets where the convergence is not monotonic, with the data of the coarsest grids spoiling the fit of the extrapolation lines.

The comparison of the error bars of the different calculations gives a good illustration of the need to estimate error bars. The direct comparison of the finest grid solutions would suggest that the results of the different grid sets are inconsistent.

Surprisingly, the BSL model with the third-order discretization of the convective terms of the k and ω transport equations exhibits a much stronger grid dependency than the equivalent C1 solution at $x = 0, y = 1.1h$.

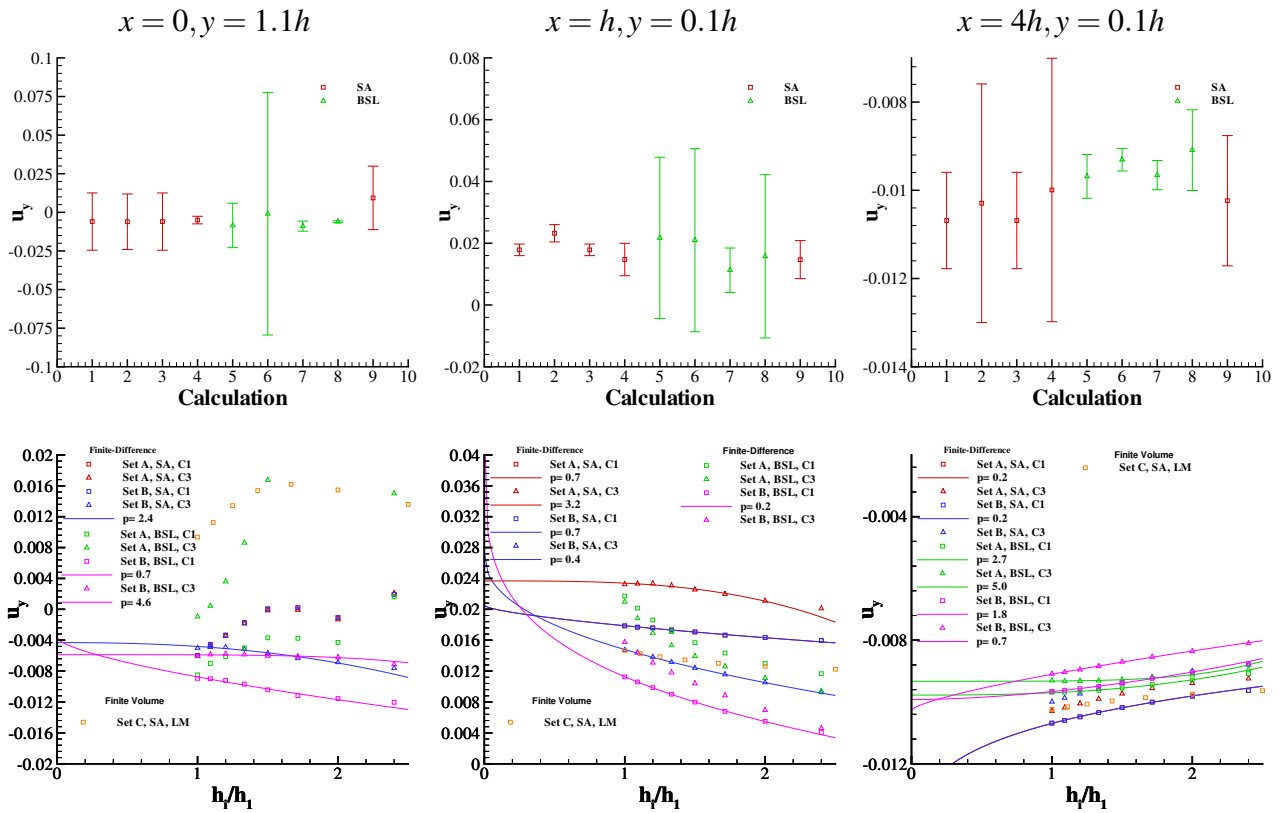


Figure 14: Convergence of u_y as a function of the grid refinement ratio at $x = 0, y = 1.1h$, $x = h, y = 0.1h$ and $x = 4h, y = 0.1h$ and respective error bars. Flow over a backward facing step.

5.5 C_p , pressure coefficient

Figure 15 presents the results obtained for the pressure coefficient, C_p , at the three selected location.

In general, the trends observed for C_p are similar to the ones discussed above for the vertical velocity component, u_y . However, most of the C_p solutions exhibit monotonic convergence. Nevertheless, the estimated values of p are within 0.2 to 4.7, which is clearly another demonstration that the data are not in the asymptotic range.

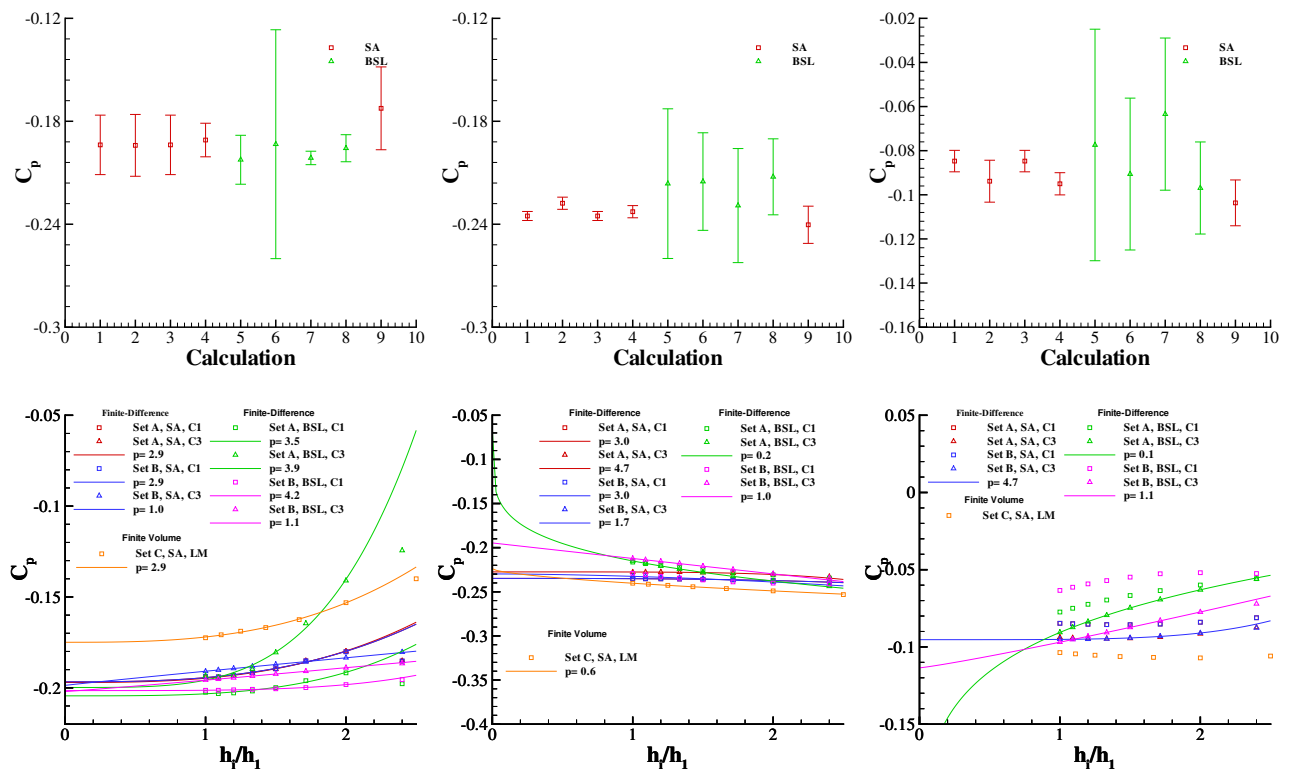


Figure 15: Convergence of C_p as a function of the grid refinement ratio at $x = 0, y = 1.1h$, $x = h, y = 0.1h$ and $x = 4h, y = 0.1h$ and respective error bars. Flow over a backward facing step.

5.6 ν_t , eddy-viscosity

Figure 16 presents the convergence of the eddy-viscosity, ν_t , as a function of the grid refinement at the three selected locations. As for the previous flow variables, the plots include also the estimated error bars for the finest grid of each set.

The results confirm the trends discussed previously for the other flow variables. However, as far as the difference between turbulence models is indicative of the modelling error, only at $x = 4h, y = 0.1h$ the differences between the values of ν_t predicted by the two turbulence models clearly exceeds the numerical uncertainty.

5.7 x_{ret} , reattachment point

Figure 17 presents the predictions of the reattachment point and the respective error bars for the finest grids of each set.

Although the grid dependence for the Spalart & Allmaras data is clearly smaller than for the BSL $k - \omega$ model, it is not possible to establish p for any of the calculations with the Spalart & Allmaras model. As for most of the previous variables, the present grid resolution leads to a significant numerical uncertainty. This is an unwelcome result, because it suggests that accurate calculation of turbulent flows requires much denser grids than the standards accepted nowadays.

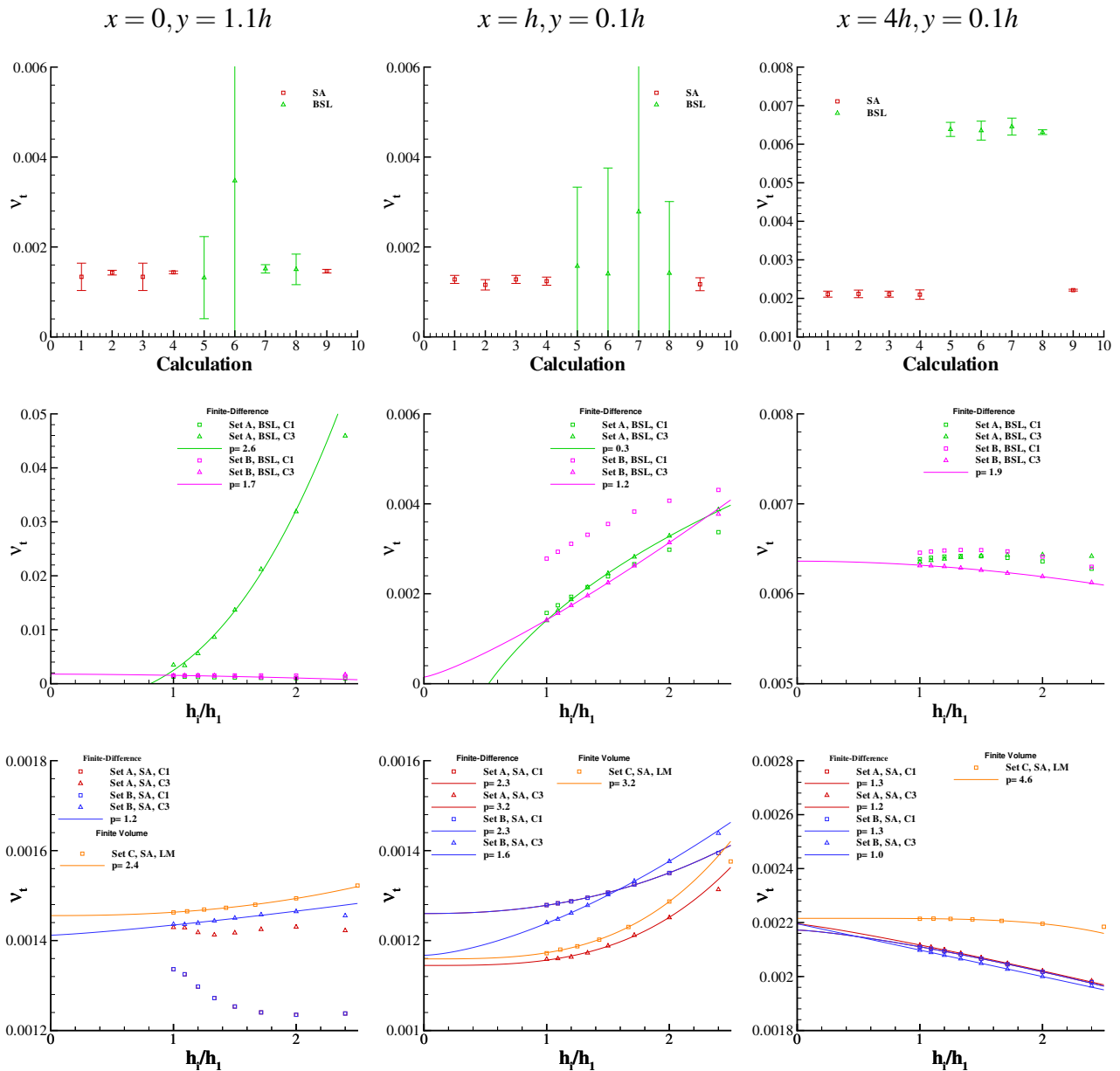


Figure 16: Convergence of v_t as a function of the grid refinement ratio at $x = 0, y = 1.1h$, $x = h, y = 0.1h$ and $x = 4h, y = 0.1h$ and respective error bars. Flow over a backward facing step.

5.8 Resistance coefficient at the walls

The friction resistance coefficient, C_F , at the top and bottom walls, and the pressure resistance coefficient at the bottom wall, C_p , are plotted in figure 18 as a function of the grid refinement.

As expected, the results obtained for the integral flow quantities are much smoother than for the local flow quantities. The observed order of accuracy is close to 1 in most of the cases and there is complete consistency between the error bars estimated for the different grid sets.

The estimated uncertainty for C_F is similar for the two turbulence models and for the C1 and C3

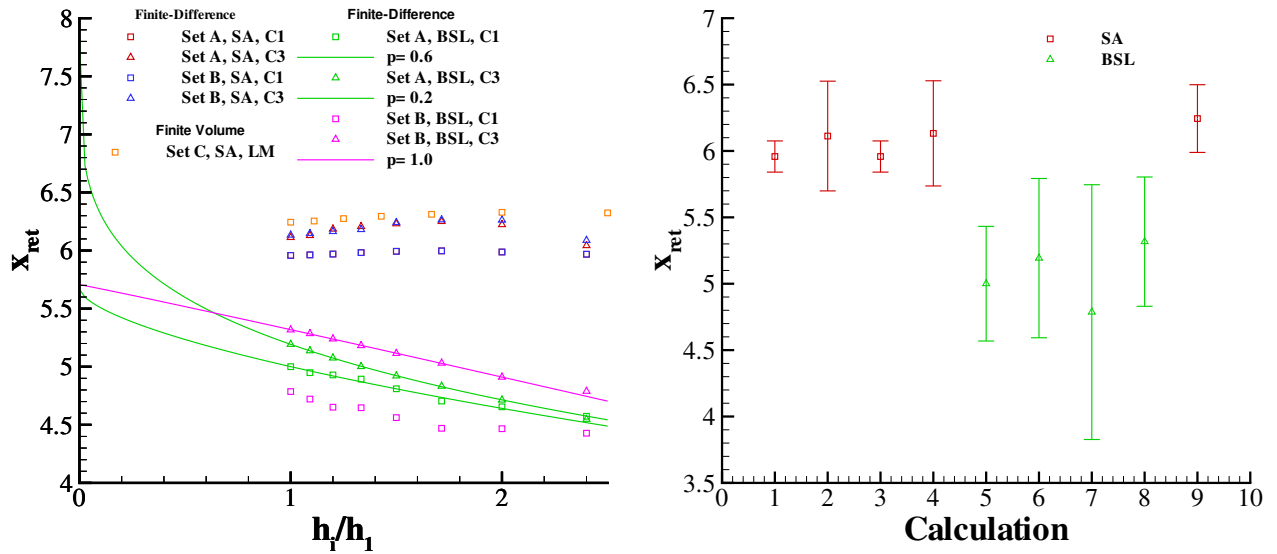


Figure 17: Convergence of the reattachment point, x_{ret} as a function of the grid refinement ratio and respective error bars. Flow over a backward facing step.

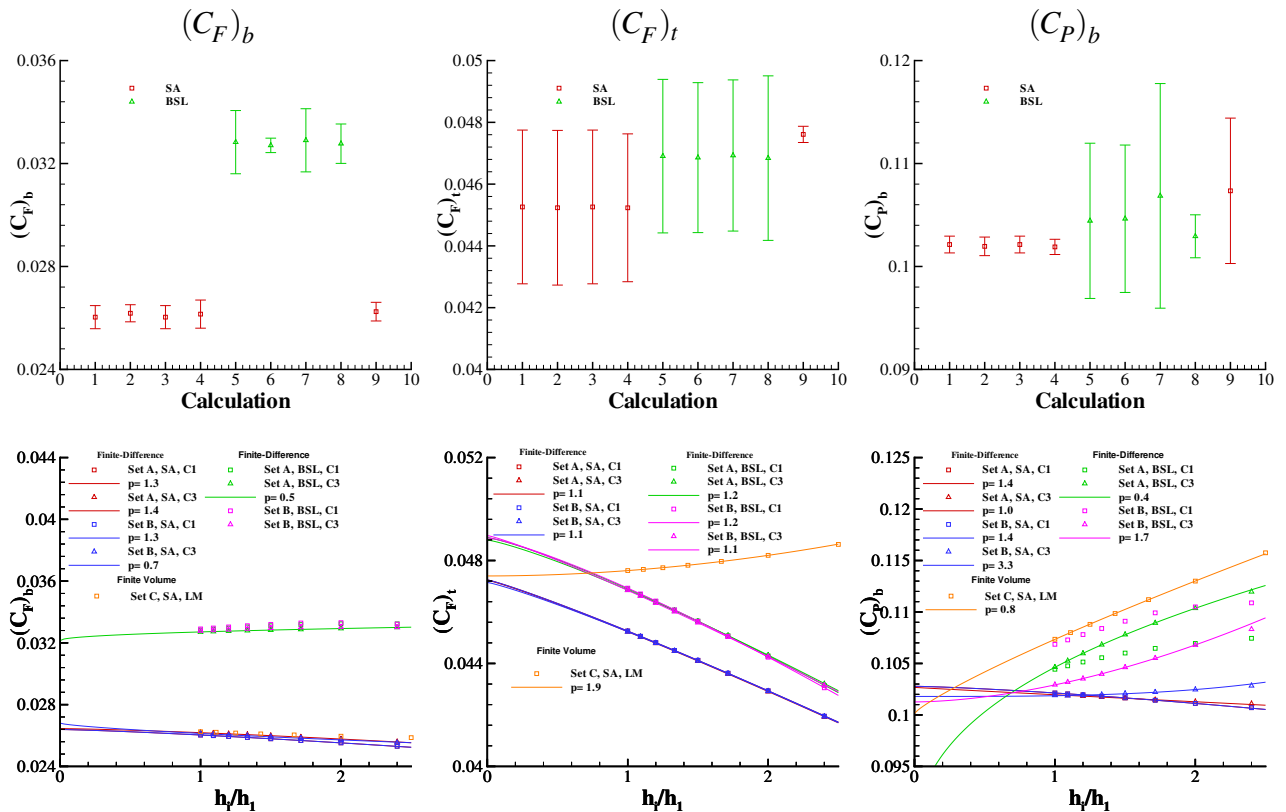


Figure 18: Convergence of the resistance coefficients at the walls, $(C_F)_b$, $(C_F)_t$ and $(C_P)_b$ as a function of the grid refinement ratio and respective error bars. Flow over a backward facing step.

calculations. The only integral parameter where the difference between the predictions of the two turbulence models is larger than the numerical uncertainty is the friction resistance at the bottom.

6 Conclusions

The present paper presents the application of a procedure to estimate the discretization uncertainty based on a least squares version of the Grid Convergence Index and on the data range to the two test cases of the 2nd Workshop on CFD Uncertainty Analysis: a manufactured solution that mimics an incompressible near-wall turbulent flow; the flow over a backward facing step taken from the ERCOFTAC Classic Database. The finite-differences and finite-volume versions of PARNASSOS have been used with the one-equation model of Spalart & Allmaras and the baseline $k - \omega$ two-equation model.

Three different exercises have been performed for the manufactured solution: calculation of the flow field with the manufactured eddy-viscosity; calculation of the eddy-viscosity field with the manufactured velocity field; calculation of the complete flow field. The results obtained in Cartesian and non-orthogonal grids suggest the following remarks:

- The theoretical order of accuracy is observed for all the flow variables when the viscosity is specified from the manufactured solution.
- The two turbulence models exhibit the theoretical order of accuracy for all the turbulence quantities when the manufactured velocity field is used with the exception of ω . The RMS of the error of ω increases with the grid refinement due to the ω wall boundary condition, ω goes to infinity. Nevertheless, the problem is local and the RMS error of ωy^2 (that remains finite at the wall) converges with second-order accuracy.
- In the complete field calculations with the Spalart & Allmaras turbulence model, the observed order of accuracy of the main flow variables is smaller than the theoretical order of the method in the region where the damping function is active. On the other hand, the results obtained with the baseline $k - \omega$ model exhibit the same behaviour obtained for the simpler exercises. Nevertheless, local flow quantities may exhibit an observed order of accuracy different from the theoretical order of the method.

The results obtained for local quantities in the flow over the backward facing step show a much less smooth convergence behaviour than the one obtained for the manufactured solution. For the level of grid refinement adopted, it is extremely difficult to establish the observed order of accuracy and there are several flow quantities that do not exhibit a monotonic convergence with the grid refinement. Nevertheless, the estimated error bars show overlap for the calculations performed with the same turbulence model in most of the cases considered.

The logical conclusion from the results obtained for the selected flow quantities is that the data are not in the asymptotic range. We are aware that this is not a popular statement, because it implies that the accurate calculation of turbulent flows with the Reynolds-Averaged Navier-Stokes equations may require much denser grid than what is commonly accepted.

The selected integral parameters, friction and pressure resistance coefficients at the walls, exhibit a much smoother convergence behaviour than the local flow quantities. This is in agreement with the experience reported also in the first Workshop on CFD Uncertainty Analysis.

References

- [1] Roache P.J. - *Verification and Validation in Computational Science and Engineering* - Hermosa Publishers, 1998.
- [2] Proceedings of the Workshop on CFD Uncertainty Analysis - Eça L, Hoekstra M. Eds., Lisbon, October 2004.
- [3] Eça L., Hoekstra M., Roache P.J. - *Verification of Calculations: an Overview of the Lisbon Workshop* - AIAA Paper 4728, AIAA Computational Fluid Dynamics Conference, Toronto, June 2005.
- [4] Eça L., Hoekstra M., Hay A., Pelletier D. - *A Manufactured Solution for a Two-Dimensional Steady Wall-Bounded Incompressible Turbulent Flow* - IST Report D72-34, EPM Report EMP-RT-2005-08, November 2005.
- [5] Eça L., Hoekstra M., Hay A., Pelletier D. - *Manufactured Solutions for One-equation Turbulence Models in a Two-Dimensional Steady Wall-Bounded Incompressible Turbulent Flow* - IST Report D72-36, EPM Report EMP-RT-2006-02, February 2006.
- [6] Eça L, Hoekstra M., *On the Influence of the Iterative Error in the Numerical Uncertainty of Ship Viscous Flow Calculations*, 26th Symposium on Naval Hydrodynamics, Rome, Italy, September 2006.
- [7] Roache P.J. - *Error Bars for CFD* - AIAA-2003-048, 41th Aerospace Sciences Meeting, Reno NV, January 2003.
- [8] Eça L, Hoekstra M. - *An Evaluation of Verification Procedures for CFD Applications* - 24th Symposium on Naval Hydrodynamics, Fukuoka, Japan, July 2002.
- [9] José M.Q.B. Jacob, Eça L. - *2-D Incompressible Steady Flow Calculations with a Fully Coupled Method* - VI Congresso Nacional de Mecânica Aplicada e Computacional, Aveiro, April 2000
- [10] Hoekstra M. - *Numerical Simulation of Ship Stern Flows with a Space-marching Navier-Stokes Method* - PhD Thesis, Delft 1999.
- [11] Spalart P.R., Allmaras S.R. - *A One-Equations Turbulence Model for Aerodynamic Flows* - AIAA 30th Aerospace Sciences Meeting, Reno, January 1992.
- [12] Menter F.R. - *Two-Equation Eddy-Viscosity Turbulence Models for Engineering Applications* - AIAA Journal, Vol.32, August 1994, pp. 1598-1605.
- [13] Saad Y, Schultz M.H. - *GMRES: a generalized minimum residual algorithm for solving non-symmetric linear systems* - SIAM Jnl. Sci. Statist. Comp., Vol. 7, pp 856-869, 1986.
- [14] Eça L., Hoekstra M. - *Verification of Turbulence Models with a Manufactured Solution* - European Conference on Computational Fluid Dynamics, ECCOMAS CFD 2006, September 2006, Netherlands.

- [15] Vinokur M. - *On One-Dimensional Stretching Functions for Finite-Difference Calculations.* - Journal of Computational Physics, Vol. 50, 1983, pp. 215-234.
- [16] Eça L., Hoekstra M., Hay A., Pelletier D. - *On the Construction of Manufactured Solutions for One and Two-Equation Eddy-Viscosity Models* - Accepted for publication in the International Journal of Numerical Methods in Fluids, Wiley, 2006.
- [17] Wilcox D.C. - *Turbulence Modeling for CFD* - DCW Industries, Second Edition, March 2000.